

Crystals for the HHCAL Detector Concept

Rihua Mao, *Member, IEEE*, Liyuan Zhang, *Member, IEEE*, and Ren-Yuan Zhu, *Senior Member, IEEE*

Abstract—Crystal calorimeter has traditionally played an important role in precision measurement of electrons and photons in high energy physics experiments. Recent interest in calorimeter technology extends its application to measurement of hadrons and jets with dual readout for both Cherenkov and scintillation light. Optical and scintillation properties of crystal scintillators commonly used in particle physics experiments are reviewed. Technologies to discriminate Cherenkov and scintillation light is elaborated. Candidate crystals for the homogeneous hadronic calorimeter detector concept and their recent development are discussed.

Index Terms—Calorimeter, crystal, dual readout, homogeneous hadronic calorimeter, scintillator.

I. INTRODUCTION

TOTAL absorption shower counters made of inorganic crystal scintillators have been known for decades for their superb energy resolution and detection efficiency for electrons and photons [1]. In high energy and nuclear physics, crystal calorimeters have been constructed, and their use has been a key factor in the successful physics programs of many experiments. The physics discovery potential of crystal calorimeter was early demonstrated by the Crystal Ball experiment through its study of radiative transitions and decays of the Charmonium family [2]. With proper calibration and monitoring, crystal calorimeters usually deliver their designed resolution *in situ* [3].

Table I summarizes parameters of past and present crystal electromagnetic calorimeters in high energy physics experiments [1]. One notes that each of these calorimeters requires several cubic meters of high quality crystals. The most ambitious crystal calorimeter is presumably the CMS calorimeter which uses 11 m^3 PbWO_4 crystals [4]. Recent interest in the homogeneous hadronic calorimeter (HHCAL) detector concept extends the application of crystals to the measurement of hadrons and jets with high resolution [5], [22]. This HHCAL detector concept adapts dual readout for both Cherenkov and scintillation light, which has been extensively studied recently by the Dream collaboration [6].

Section II of this paper describes the optical and scintillation properties of heavy crystal scintillators commonly used in par-

ticle physics experiments. Discrimination between Cherenkov and scintillation light is discussed in Section III. Section IV discusses candidate crystals for the HHCAL detector concept. A brief summary is given in Section V.

II. PROPERTIES OF CRYSTAL SCINTILLATORS

Table II [7] lists the basic properties of heavy crystals with mass production capability: NaI(Tl) , CsI(Tl) , BaF_2 , CeF_3 , bismuth germanate ($\text{Bi}_4\text{Ge}_3\text{O}_{12}$ or BGO), lead tungstate (PbWO_4 or PWO), LSO [8]/LYSO [9], [23] and PbF_2 . All, except PbF_2 , are scintillators with the characteristics of their scintillation light listed. All, except CeF_3 , have either been used in, or actively being pursued for, high energy and nuclear physics experiments, which are also listed in the table. The experiment name in bold indicates possible future crystal calorimeters in the next decade. LSO and LYSO crystals are also widely used in the medical industry. Mass production capabilities exist for all these crystals.

Fig. 1 is a photo showing twelve crystal scintillator samples. In addition to samples listed in Table II pure CsI , CsI(Na) , LYSO as well as LaCl_3 and LaBr_3 [10] are also shown in this photo although the last two are not yet in a mass production stage. Samples are arranged in an order of their density, or radiation length. All non-hygroscopic samples are wrapped with white Tyvek paper as reflector. Hygroscopic NaI , CsI , LaBr_3 and LaCl_3 are sealed in a package with two ends made of quartz windows of 3 or 5 mm thickness to avoid surface degradation. To minimize uncertainties in the light output measurement caused by the sample size dependence all samples have a cubic shape of $1.5 \times 1.5 \times 1.5 X_0^3$, except NaI(Tl) and LaCl_3 which are a cylinder with a length of $1.5 X_0$ and areas at two ends equaling to $1.5 \times 1.5 X_0^2$ to match the 2 inch diameter of the PMT cathode.

Fig. 2 shows a comparison of the transmittance, photo-luminescence and excitation spectra for ten samples. The solid black dots in these plots are the theoretical limit of the transmittance, which is calculated using the corresponding refractive index as a function of wavelength taking into account multiple reflections between the two parallel end surfaces and assuming no internal absorption [11]. Most samples, except LaBr_3 and LaCl_3 , have their transmittance approaching the theoretical limits, indicating negligible internal absorption. The poor transmittance measured for LaBr_3 and LaCl_3 samples is probably due to scattering centers inside these samples. It is interesting to note that BaF_2 , BGO, NaI(Tl) , CsI(Tl) and PbWO_4 have their emission spectra well within the transparent region showing no obvious self-absorption effect. The UV absorption edge in the transmittance spectra of LSO, LYSO, CeF_3 , LaBr_3 and LaCl_3 , however, cuts into the emission spectra and thus affects crystal's light output. This self-absorption effect is more serious in long crystal samples used in high energy and nuclear physics experiment as extensively discussed for LSO and LYSO crystals [12], [13]. We also note that the values of the cut-off wavelength, at which

Manuscript received November 16, 2011; revised January 18, 2012; accepted February 28, 2012. Date of publication May 03, 2012; date of current version October 09, 2012. This work was supported in part by the U.S. Department of Energy under grant DE-FG03-92-ER-40701 and the U.S. National Science Foundation Award PHY-0612805.

The authors are with the California Institute of Technology, Pasadena, CA 91125 USA (e-mail: zhu@hep.caltech.edu).

Color versions of one or more of the figures in this paper are available online at <http://ieeexplore.ieee.org>.

Digital Object Identifier 10.1109/TNS.2012.2192290

TABLE I
CRYSTAL CALORIMETER IN HIGH ENERGY PHYSICS: PAST AND PRESENT

Experiment	C. Ball	L3	CLEO II	C. Barrel	KTeV	BaBar	BELLE	CMS
Accelerator	SPEAR	LEP	CESR	LEAR	Tevatron	PEP II	KEK	LHC
Date	75–85	80–00	80–00	85–95	90–10	94–10	94–10	95–20
Crystal Type	NaI(Tl)	BGO	CsI(Tl)	CsI(Tl)	CsI	CsI(Tl)	CsI(Tl)	PbWO ₄
B-Field (Tesla)	-	0.5	1.5	1.5	-	1.5	1.0	4.0
Inner Radius (m)	0.254	0.55	1.0	0.27	-	1.0	1.25	1.29
Number of Crystals	672	11,400	7,800	1,400	3,300	6,580	8,800	76,000
Crystal Depth (X ₀)	16	22	16	16	27	16 to 17.5	16.2	25
Crystal Volume (m ³)	1	1.5	7	1	2	5.9	9.5	11
L. Yield (p.e./MeV)	350	1,400	5,000	2,000	40	5,000	5,000	2
Photo-sensor	PMT	Si PD	Si PD	WS [†] + Si PD	PMT	Si PD	Si PD	APD [‡]
Photo-sensor Gain	Large	1	1	1	4,000	1	1	50
Noise/Can. (MeV)	0.05	0.8	0.5	0.2	Small	0.15	0.2	30
Dynamic Range	10 ⁴	10 ⁵	10 ⁴	10 ⁴	10 ⁴	10 ⁴	10 ⁴	10 ⁵

[†] Wavelength Shifter.

[‡] Avalanche photo-diode.

TABLE II
PROPERTIES OF HEAVY CRYSTAL WITH MASS PRODUCTION CAPABILITY

Crystal	NaI(Tl)	CsI(Tl)	CsI	BaF ₂	CeF ₃	BGO	PbWO ₄	LSO/LYSO(Ce)	PbF ₂
Density (g/cm ³)	3.67	4.51	4.51	4.89	6.16	7.13	8.3	7.40	7.77
Melting Point (°C)	651	621	621	1280	1460	1050	1123	2050	824
Radiation Length (cm)	2.59	1.86	1.86	2.03	1.70	1.12	0.89	1.14	0.93
Molière Radius (cm)	4.13	3.57	3.57	3.10	2.41	2.23	2.00	2.07	2.21
Interaction Length (cm)	42.9	39.3	39.3	30.7	23.2	22.7	20.7	20.9	21.0
Refractive Index ^a	1.85	1.79	1.95	1.50	1.62	2.15	2.20	1.82	1.82
Hygroscopicity	Yes	Slight	Slight	No	No	No	No	No	No
Luminescence ^b (nm)	410	560	420	300	340	480	425	420	?
(at Peak)			310	220	300		420		
Decay Time ^b (ns)	245	1220	30	650	30	300	30	40	?
			6	0.9			10		
Light Yield ^{b,c}	100	165	3.6	36	7.3	21	0.30	85	?
			1.1	4.1			0.077		
d(LY)/dT ^{b,d} (%/°C)	-0.2	0.4	-1.4	-1.9	~0	-0.9	-2.5	-0.2	?
				0.1					
Experiment	Crystal Ball	CLEO BaBar BELLE BES III	KTeV	TAPS	-	L3 BELLE	CMS ALICE PrimEx Panda	Mu2e SuperB HL-LHC?	A4 HHCAL?

a At the wavelength of the emission maximum.

b Top line: slow component, bottom line: fast component.

c Relative light yield of samples of 1.5 X₀ and with the PMT quantum efficiency taken out.

d At room temperature.

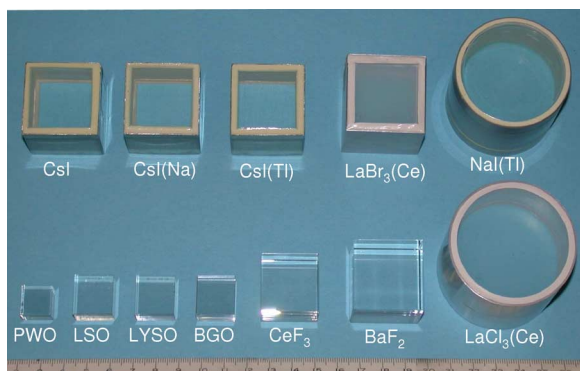


Fig. 1. A photo shows twelve crystal scintillators with dimension of 1.5 X₀.

the transmittance data show 50% of that at 800 nm, are 140 nm, 280 nm, 293 nm, 315 nm, 318 nm, 342 nm, 358 nm, 365 nm and 390 nm for BaF₂, CsI, CeF₃, BGO, CsI(Na), PWO, CsI(Tl), NaI(Tl) and LSO/LYSO respectively. On the other hand it is 250 nm for PbF₂, indicating that it is a good Cherenkov radiator.

Fig. 3 shows the ¹³⁷Cs γ -ray pulse height spectra measured by a Hamamatsu R1306 PMT with a bi-alkali cathode for twelve crystal samples. Also shown in these figures are the corresponding FWHM energy resolution (E.R.), which is affected by the quantum efficiency of the readout device. γ -ray spectroscopy with a few percents resolution is required to identify isotopes for the homeland security applications. It is clear that only LaBr₃ approaches this requirement. All other crystals do not provide sufficient energy resolution at low energies.

Figs. 4 and 5 show light output in photo-electrons per MeV energy deposition as a function of the integration time, measured using a Photonic XP2254b PMT with a multi-alkali photo cathode, for six fast crystal scintillators: LaBr₃, LSO, LYSO, CeF₃, un-doped CsI and PbWO₄ and six slow crystal scintillators: NaI(Tl), CsI(Na), CsI(Tl), LaCl₃, BaF₂ and BGO. The corresponding fits to the exponentials and their numerical results are also shown in these figures. The un-doped CsI, PbWO₄, LaCl₃ and BaF₂ crystals are observed to have two decay components. Despite its poor transmittance the cerium doped LaBr₃ is

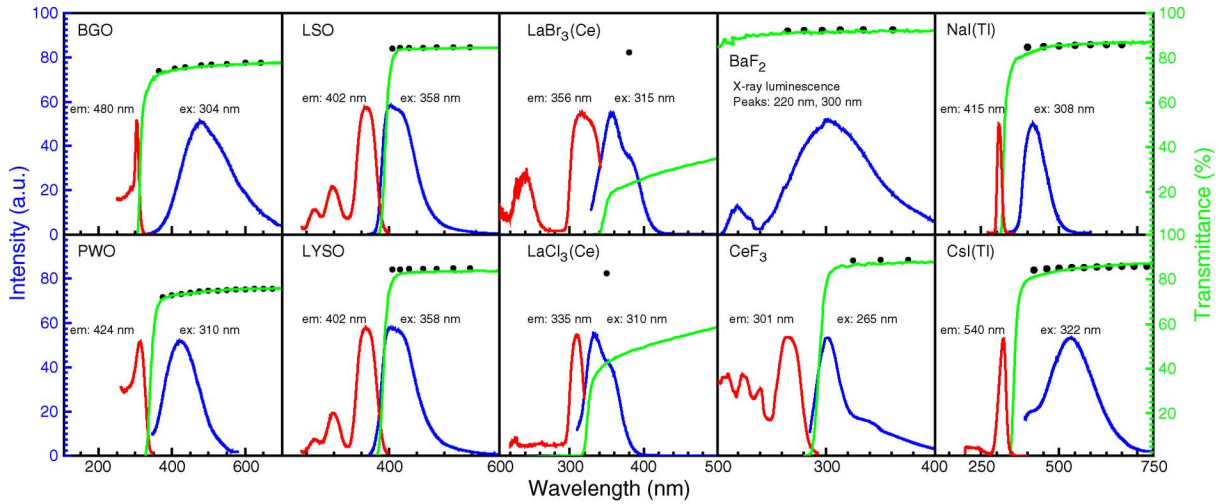


Fig. 2. The excitation (red) and emission (blue) spectra (left scale) and the transmittance (green) spectra (right scale) are shown as a function of wavelength for ten crystal scintillators. The solid black dots are the theoretical limit of the transmittance.

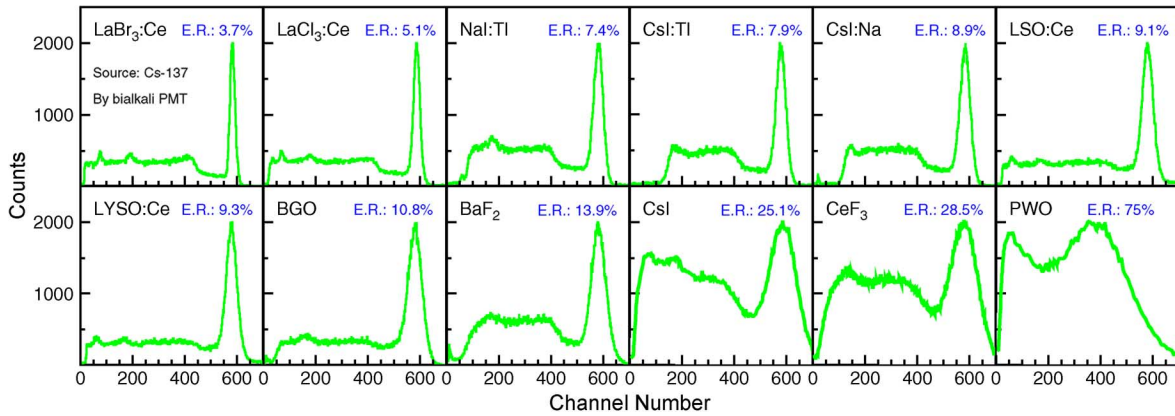


Fig. 3. ^{137}Cs γ -ray pulse height spectra measured by a Hamamatsu R1306 PMT are shown for twelve crystal samples. The numerical values of the FWHM resolution (E.R.) are also shown in the figure.

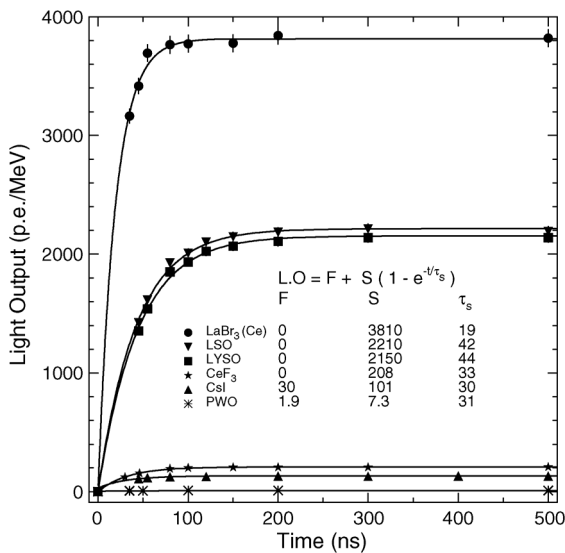


Fig. 4. Light output measured using a XP2254b PMT is shown as a function of integration time for six fast crystal scintillators.

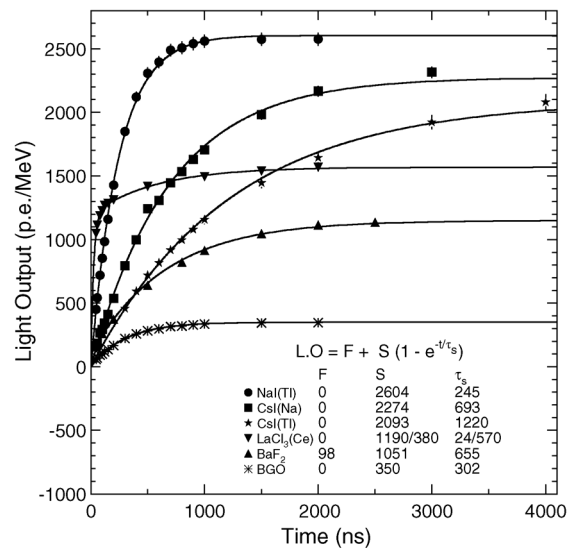


Fig. 5. Light output measured using a XP2254b PMT is shown as a function of integration time for six slow crystal scintillators.

distinguished by its bright fast scintillation, leading to the excellent energy resolution for the γ -ray spectroscopic applications. The LSO and LYSO samples have a consistent fast decay time

(~ 40 ns) and photo-electron yield, which is 6 and 230 times of BGO and PbWO_4 respectively.

Since the quantum efficiency of the PMT used for the light output measurement is a function of wavelength, it should be

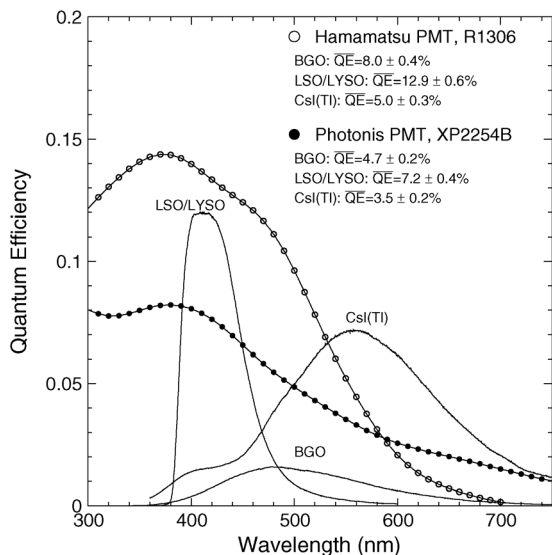


Fig. 6. Quantum efficiencies of a Hamamatsu 1306 PMT with a bi-alkali cathode (open circles) and a Photonis 2254B PMT with a multi-alkali cathode (solid dots) are shown as a function of wavelength together with the emission spectra of the LSO/LYSO, BGO and CsI(Tl) samples, where the area under the emission curves is proportional to their corresponding absolute light output.

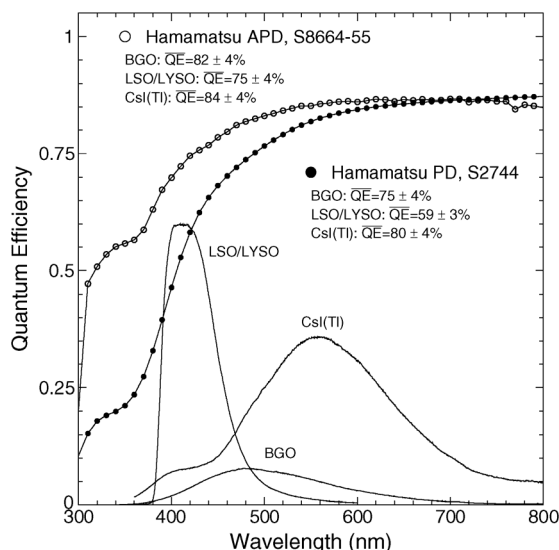


Fig. 7. The same as Fig. 6 for a Hamamatsu S8664 Si APD (open circles) and a Hamamatsu S2744 Si PIN diode (solid dots).

corrected for to directly compare the light output between different crystals. Figs. 6 and 7 show the typical quantum efficiency as a function of wavelength for a PMT with a bi-alkali cathode (Hamamatsu R1306) and a PMT with a multi-alkali cathode (Photonis 2254B), a Si APD (Hamamatsu S8664) and a Si PIN PD (Hamamatsu S2744). The emission spectra of LSO/LYSO, BGO and CsI(Tl) crystals are also shown in these figures. The light output values listed in Table II are corrected for the PMT quantum efficiency. The light output of LSO and LYSO crystals is a factor of 4 and 200 of that of BGO and PbWO₄ respectively.

The scintillation light yield of crystals may also depend on temperature. Fig. 8 shows the light output variations for twelve crystal samples between 15°C and 25°C. The corresponding temperature coefficients obtained from linear fits are also listed

in the figure. The numerical result of these fits is also listed in Table II.

III. DISCRIMINATION BETWEEN CHERENKOV AND SCINTILLATION LIGHT

Crystals have recently been proposed to construct a homogeneous calorimeter, including both electromagnetic and hadronic components [5], [22]. This HHCAL detector concept removes the traditional boundary between ECAL and HCAL, thus eliminating the effect of dead materials in the middle of the hadronic shower development. It takes advantage of the recently implemented dual readout approach to measure both Cherenkov and scintillation light to achieve good energy resolution for hadronic jet measurements [6]. Because of the unprecedented volume (70 to 100 m³) foreseen for such a calorimeter [5], [22], the crystal material must be dense (to reduce the volume), UV transparent (to effectively collect the Cherenkov light) and allows a clear discrimination between the Cherenkov and scintillation light.

Fig. 9 shows samples of three 5 × 5 × 5 cm³ crystal samples: PbF₂, BGO and PWO. Crystals of this size can be seen as typical building block for a crystal hadronic calorimeter. All material are dense with a nuclear interaction length in a range from 21 cm (PWO and PbF₂) to 23 cm (BGO).

Fig. 10 shows the transmittance spectra of PbF₂ (green), BGO (blue), PWO (red) and a UG11 filter (black) as a function of wavelength together with the Cherenkov emission spectrum (dashed blue). The UG 11 filter can be used to select the Cherenkov light with little or no scintillation contamination. Also shown in this figure is the normalized figure of merit for the Cherenkov measurement using the UG11 filter, which is defined as the transmittance weighted Cherenkov emission spectrum (TWEM). Their numerical values are 1.0:0.53:0.21, which would be 1.0:0.82:0.75 without the UG11 filter. Among these materials PbF₂ is the most efficient in collecting the Cherenkov light because of its good UV transmission.

An effective technology to discriminate Cherenkov and scintillation light can be realized using an optical filter or pulse timing. Fig. 11 shows a set-up used to investigate Cherenkov light collection and its discrimination from the scintillation light. Samples shown in Fig. 9 were used in this investigation. To avoid the multiple light reflection effect all crystals were wrapped with black paper. Cosmic-rays were triggered by two finger counters with coincidence. The Cherenkov and scintillation light pulses generated by cosmic-rays were measured simultaneously by two Hamamatsu R2059 PMT coupled to the sample through optical filters UG11 and GG400. GG400 is a low-pass filter with cut-off at 400 nm. The UG11 filter is used to select the Cherenkov light as shown in Fig. 10. The GG400 filter is used to select the scintillation light with small contamination of the Cherenkov light. The output of these two PMTs were digitized by an Agilent 6052A digital scope.

Fig. 12 shows the front edge of the scintillation light pulse from BGO and PWO, observed through the GG400 filter. Their delay from the trigger (t_d) and rise time (t_r) are identical with numerical values of 6.2 ns and 1.9 ns respectively with the later dominated by the rise time of DSO (0.7 ns) and PMT (1.3 ns). Fig. 13 shows the Cherenkov light pulse shape observed for PbF₂ (Left), BGO (Middle) and PWO (Right) through the UG11

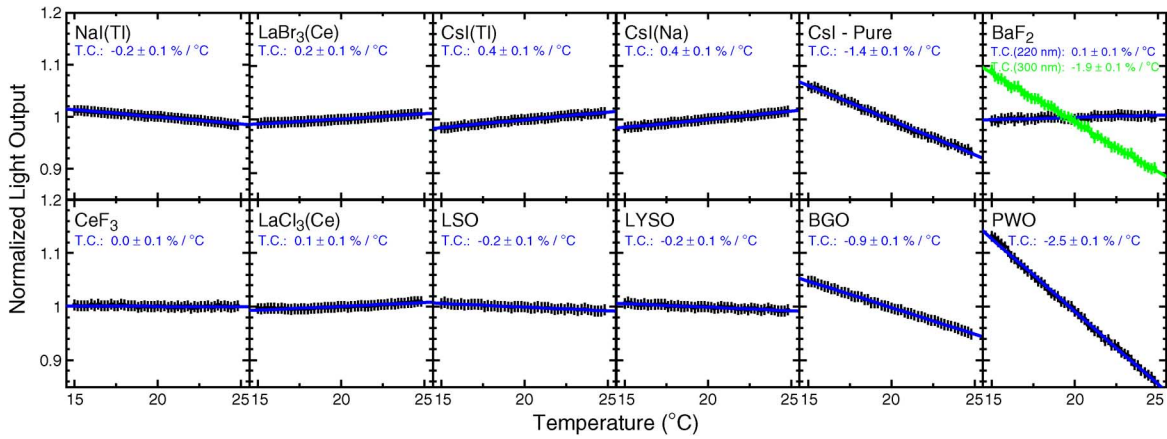


Fig. 8. Light output temperature coefficient obtained from linear fits between 15°C and 25°C for twelve crystal scintillators.

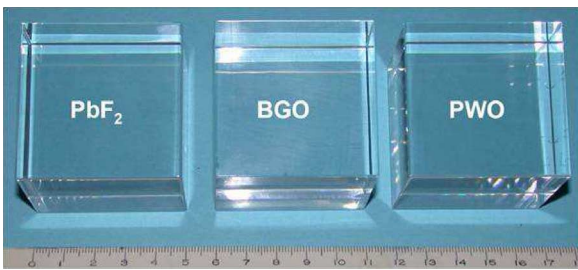


Fig. 9. A photo shows three crystal samples of $5 \times 5 \times 5 \text{ cm}^3$ investigated for the homogeneous hadronic calorimeter concept.

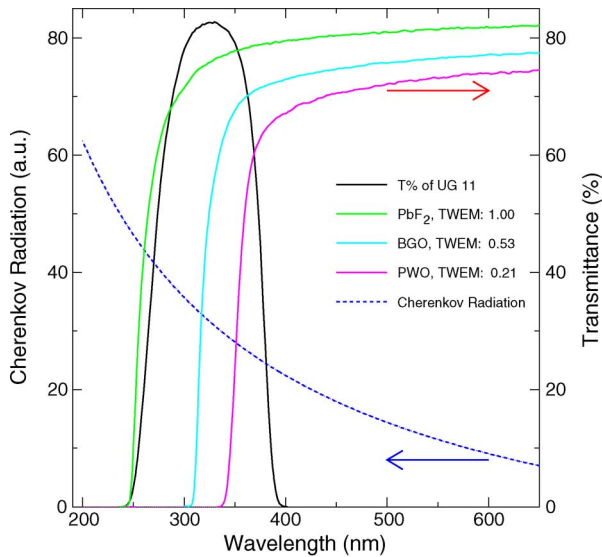


Fig. 10. The transmittance spectra of PbF₂ (green), BGO (blue), PWO (red) and UG11 (black) are shown as a function of wavelength. Also shown in this figure are the Cherenkov emission spectrum (dashed blue) and the normalized figure of merit for the Cherenkov light measurement with the UG11 filter.

filter. All pulses have a consistent time structure in the delay (6.1 ns), the rise time (1.8 ns), the fall time (4.2 ns) and the FWHM width (3.0 ns). It is interesting to note that there is actually no difference observed in the delay and rise time between the Cherenkov and scintillation light, indicating that only the light pulse width and fall time are useful for the discrimination

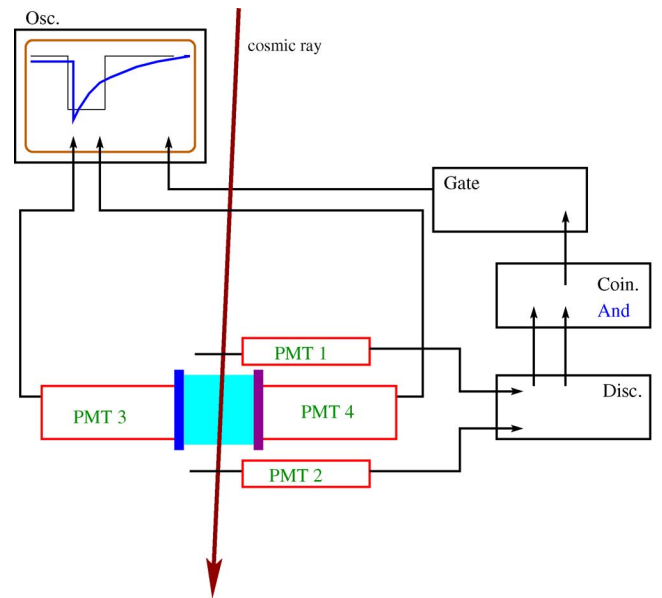


Fig. 11. A schematic showing a simple set-up used to measure cosmic-ray generated Cherenkov and scintillation light simultaneously using two Hamamatsu R2059 PMTs.

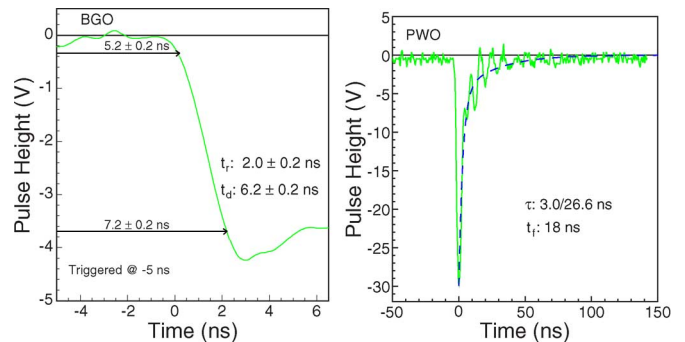


Fig. 12. The light pulses are recorded by an Agilent 6052A digital scope. Digital scope traces of the scintillation light front edge measured by a Hamamatsu R2059 PMT with GG400 filter for the BGO (Left) and PWO (Right) samples.

between the Cherenkov and scintillation light. A slow scintillator may actually help this discrimination.

Because of the difference in the spectrum and direction between the Cherenkov and scintillation light the multiple reflections inside crystals may cause a difference in the measured rise time between Cherenkov and scintillation light. Fig. 14 shows

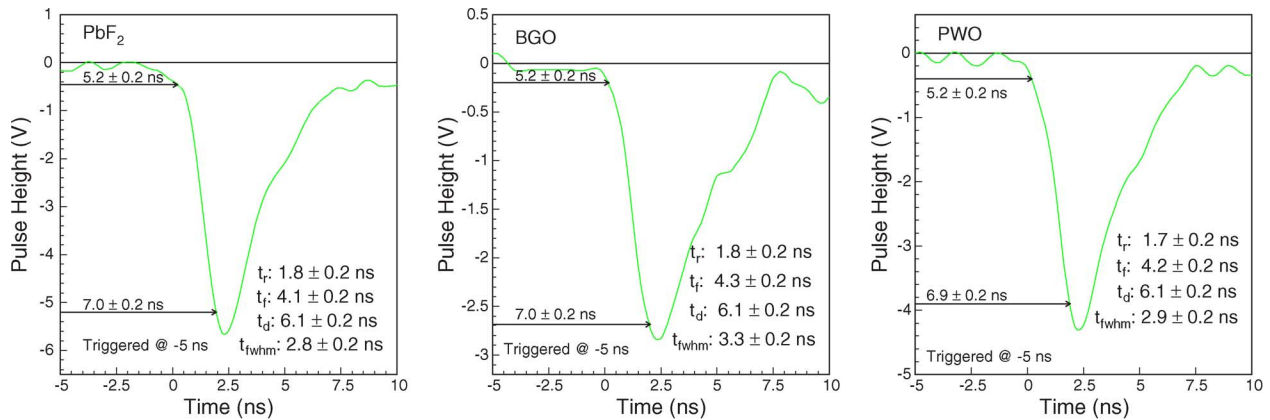


Fig. 13. Digital scope traces of Cherenkov light pulse measured by a Hamamatsu R2059 PMT with UG11 filter for the PbF₂ (Left), BGO (Middle) and PWO (Right) samples.

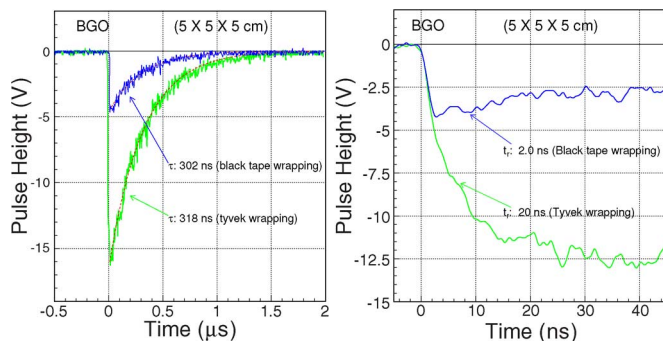


Fig. 14. Agilent 6052A digital scope traces of the scintillation light for the BGO sample with Tyvek (green) and black (blue) wrappings are shown with long (left) and short (right) time scales.

DSO traces of scintillation light for the BGO sample with different wrappings (green: Tyvek and blue: black). The multiple reflections introduced by white Tyvek paper wrapping clearly increase the measured scintillation decay time (left) and rise time (right).

The ratio of Cherenkov versus scintillation light was measured to be 1.55% and 22% for BGO and PWO respectively. These values are consistent with the scintillation light yield shown in Table II, the emission weighed quantum efficiency of the bi-alkali cathode of the Hamamatsu R2059 PMT shown in Fig. 6 and the TWEM values shown in Fig. 10.

IV. CRYSTALS FOR THE HHCAL DETECTOR CONCEPT

Based upon our experience accumulated in building electromagnetic calorimeters, an initial detector design with a pointing geometry was proposed. It may provide better resolutions for both energy and position measurements, and thus a good jet mass reconstruction. Fig. 15 shows a schematic of a typical HHCAL cell with a pointing geometry [14]. It is similar to a typical calorimeter cell of a crystal ECAL, but has several longitudinal segments with a total length of about 1 m. By using dense active materials such detector depth would provide about 5 nuclear interaction lengths, adequate for hadronic jet energy reconstruction. The readout devices are mounted on the side faces of these crystal segments. Due to the recent development in compact solid state readout devices, e.g., silicon PMTs, such a readout scheme is now feasible.

Because of the huge volume required for an HHCAL detector, development of cost-effective materials is crucial. Table III summarized the basic properties of candidate crystals being considered for this detector concept, where two crystal cost drivers, melting point and raw material cost, are also listed. While BGO may be the best material to be used for such a calorimeter its mass production cost is prohibitively high. While PWO, PbF₂, PbFCl and BSO are under investigation, PbF₂ and PbFCl are preferred because of their low melting point and raw material cost.

R&D is actively being pursued by the high energy physics community in collaboration with the material science community to search for adequate materials for the HHCAL detector concept. One approach is to develop scintillating PbF₂ crystals by selective doping. Observations of fast scintillation in Gd doped PbF₂ crystals were reported early by Shen and Woody [15], [16]. Our investigation shows that rare earth doping introduces scintillation in PbF₂, but not at the level can be measured by using a γ -ray source [17]. Fig. 16 shows the excitation, photo-luminescence and x-luminescence spectra for Er, Eu, Gd, Ho, Pr, Sm and Tb doped PbF₂ crystal samples. It is noted that some of this scintillation light is between 500 to 600 nm, which is desirable for Cherenkov/scintillation discrimination.

The photo-luminescence decay time constant of these doped PbF₂ samples was measured using a pulsed laser as the excitation source. Fig. 17 shows the photo-luminescence pulse shape (blue circles), the corresponding exponential fit (red lines) and the decay time constant for the PbF₂ samples doped with Er, Ho, Eu, Sm and Tb as well as a reference CsI(Tl) sample. The photoluminescence intensity of PbF₂ samples doped with Pr and Gd are too weak to be useful to extract the decay time constant. Table IV summarizes the decay time constants for the PbF₂ samples doped with Er, Ho, Eu, Sm and Tb. They were found at a millisecond scale as expected from the f-f transition of these rare earth elements [18], [24]. These time constants are too long to be useful for high energy physics experiments.

In a brief summary, the combination of potential low cost, good UV transmittance and mass production capability makes PbF₂ crystals a favored material for the HHCAL detector concept. Our search for scintillation found consistent photo- and x-ray luminescence spectra in PbF₂ samples doped with Er, Eu, Gd, Ho, Pr, Sm and Tb with decay time at a millisecond

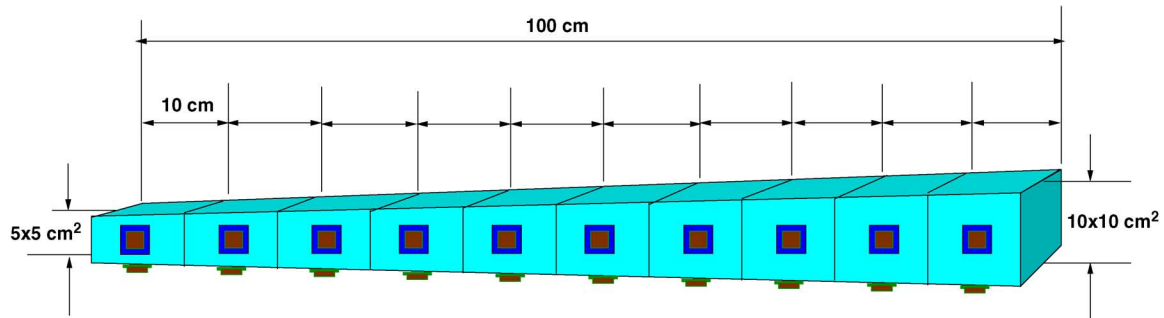


Fig. 15. A schematic showing a typical cell for the HHCAL detector concept with a pointing geometry [14].

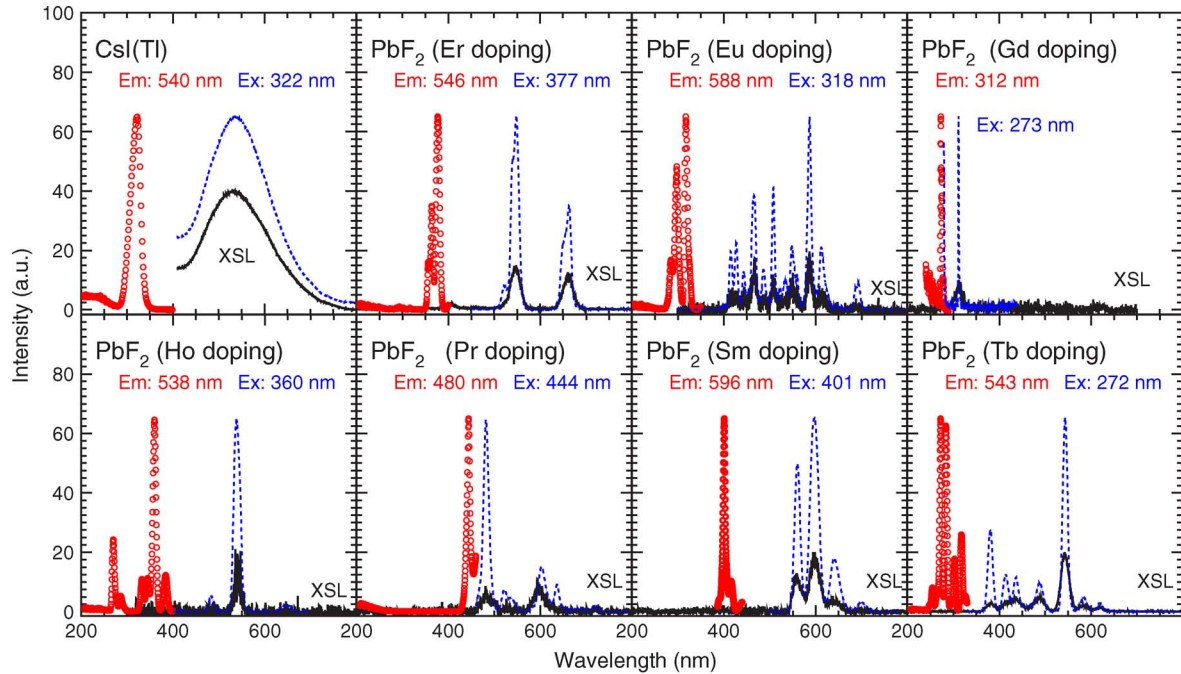

 Fig. 16. The excitation (red dots) and Photo-(blue dashes) and X-(black lines) luminescence spectra are shown as a function of wavelength for the PbF_2 samples doped with Er, Eu, Gd, Ho, Pr, Sm and Tb as well as a reference CsI(Tl) sample.

 TABLE III
 CANDIDATE CRYSTALS FOR THE HHCAL DETECTOR CONCEPT

Parameters	BGO	PWO	PbF_2	PbFCl	BSO
Density (g/cm^3)	7.13	8.29	7.77	7.11	6.8
λ_I (cm)	22.8	20.7	21.0	24.3	23.1
$n @ \lambda_{max}$	2.15	2.20	1.82	2.15	2.06
τ_{decay} (ns)	300	30/10	?	30	100
λ_{max} (nm)	480	425/420	?	420	470
Cut-Off λ (nm)	310	350	250	280	300
Light Output (%)	100	1.4/0.37	?	17	20
Melting Point ($^{\circ}\text{C}$)	1050	1123	842	608	1030
Raw Material Cost (%)	100	49	29	29	47

scale. While some Eu doped samples show γ -ray induced anode photo-current larger than the undoped samples, the numerical result indicates that the scintillation light, if any, is less than 3 p.e./MeV measured by a PMT with a bi-alkali photo-cathode. Their ^{137}Cs γ -ray excited pulse height spectra measured with up to a 10 μs integration time were also found identical to that of the undoped sample, confirming that their luminescence is too weak to show a peak. Investigation will continue to search for scintillation in doped PbF_2 phases and mixtures.

On the other hand, R&D is also actively being pursued by the material science community [19]. One other approach worthwhile to mention is to develop PWO crystals with a slow scintillation emission. Green (560 nm) and slow emission with a few μsec decay time was observed by selective doping in PWO crystals [20]. Such crystals were reported to have a factor of ten more light than yttrium doped PWO crystals used in high energy physics experiment. This slow and green scintillation would be desirable for this application. Additional approaches are also being pursued, such as PbFCl , BSO, BSO glasses and various ceramics [21].

V. SUMMARY

Precision crystal electromagnetic calorimeters have been an important part of high energy physics detectors. The availability of mass production capability of large size LSO and LYSO crystals provides an opportunity to build a LSO/LYSO crystal electromagnetic calorimeter with good energy resolution over a large dynamic range down to the MeV level. Such a calorimeter, if built, would greatly enhance the physics discovery potential for high energy and nuclear physics experiments in the next decade.

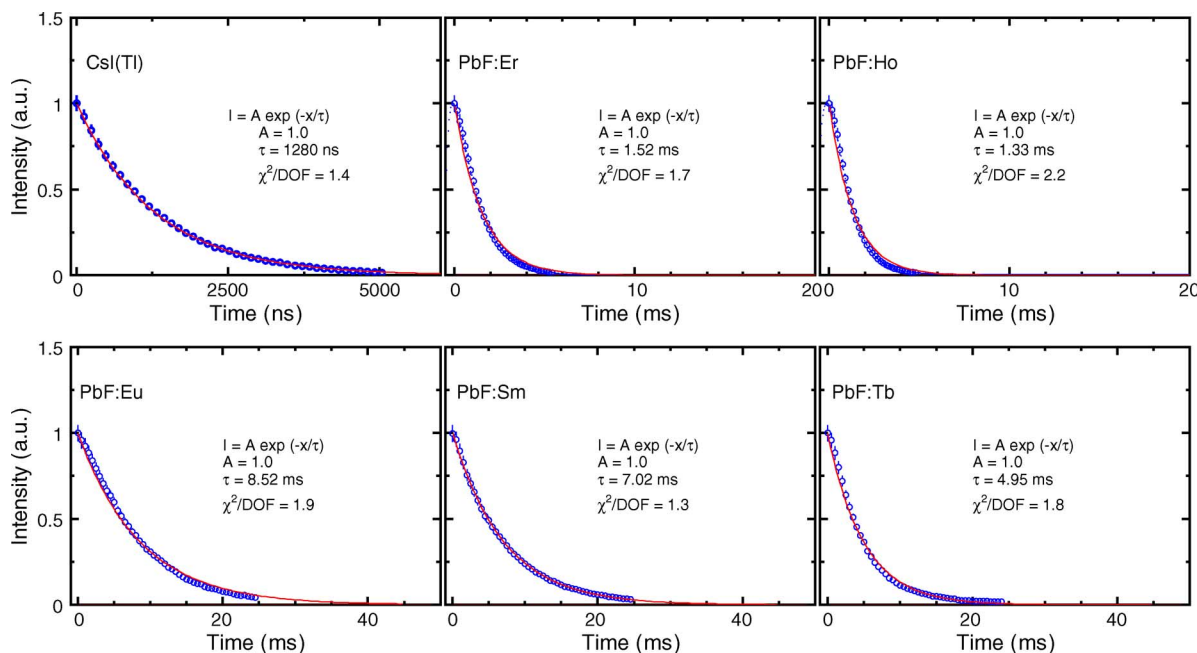


Fig. 17. The photo-luminescence pulse shape (blue circles), corresponding fit to an exponential (red lines) and the decay time constant are shown for the PbF₂ samples doped with Er, Ho, Eu, Sm and Tb as well as a reference Csl(Tl) sample.

TABLE IV
DECAY TIME CONSTANT FOR DOPED LEAD FLUORIDE CRYSTALS

Dopant	Er	Eu	Ho	Sm	Tb
Decay time constant (ms)	1.5	8.5	1.3	7.0	5.0

Recent interest in the high energy physics community to pursue a homogeneous hadronic calorimeter with dual readout opens a new area of crystal calorimetry to achieve good energy resolution for hadronic jet measurements in the next decade. The main challenge for this concept is to develop cost effective heavy scintillators with good UV transmission and excellent Cherenkov/scintillation discrimination. Dense crystals, scintillating glasses and ceramics offer a very attractive implementation for this detector concept.

ACKNOWLEDGMENT

The crystals samples used in this investigation are provided by Professors Guohao Ren, Shaohua Wang, and Hui Yuan of Shanghai Institute of Ceramics, and Prof. Dingzhong Shen of Scintibow.

REFERENCES

- [1] G. Gratta, H. Newman, and R.-Y. Zhu, "Crystal calorimeters in Particle Physics," *Annu. Rev. Nucl. Part. Sci.*, vol. 44, pp. 453–500, 1994.
- [2] E. Bloom and C. Peck, *Ann. Rev. Nucl. Part. Sci.*, vol. 33, pp. 143–197, 1983.
- [3] R.-Y. Zhu, "Calibration and monitoring for crystal calorimetry," *Nucl. Instr. and Meth.*, vol. A537, pp. 344–348, 2005.
- [4] The CMS Electromagnetic Calorimeter Project, CERN/LHCC 97-33, 1997.
- [5] A. Para, Very High Resolution Hadron Calorimetry, FERMILAB-CONF-11-519-CD.
- [6] N. Akchurin *et al.*, "Separation of crystal signals into scintillation and Cherenkov components," *Nucl. Instrum. Meth.*, vol. A537, p. 537, 2005.
- [7] R. H. Mao, L. Y. Zhang, and R.-Y. Zhu, "Optical and scintillation properties of inorganic scintillators in high energy physics," *IEEE Trans. Nucl. Sci.*, vol. 55, no. 4, pp. 2425–2431, Aug. 2008.
- [8] C. Melcher, "Lutetium orthosilicate single crystal scintillator detector," U.S. Patent 4,958,080, 1990, and 5025151 (1991).
- [9] D. W. Cooke, K. J. McClellan, B. L. Bennett, J. M. Roper, M. T. Whittaker, and R. E. Muenchausen, "Crystal growth and optical characterization of cerium-doped $Lu_{1.8}Y_{0.2}SiO_5$," *J. Appl. Phys.*, vol. 88, p. 7360, 2000.
- [10] E. Loeff, P. Dorenbos, E. Eijk, K. Kraemer, and H. Guedel, "Scintillation properties of $LaBr_3 : Ce^{3+}$ crystals: Fast efficient and high-energy resolution scintillators," *Nucl. Instrum. Meth.*, vol. A486, p. 254, 2002.
- [11] D. A. Ma and R.-Y. Zhu, "Light attenuation length of barium fluoride crystals," *Nucl. Instrum. Meth.*, vol. A333, pp. 422–424, 1993.
- [12] J. M. Chen, R. H. Mao, L. Y. Zhang, and R.-Y. Zhu, "Large size LSO and LYSO crystals for future high energy physics experiments," *IEEE Trans. Nucl. Sci.*, vol. 54, no. , pp. 3133–3140, 2007.
- [13] J. M. Chen, R. H. Mao, L. Y. Zhang, and R.-Y. Zhu, "Gamma-ray induced radiation damage in large size LSO and LYSO crystal samples," *IEEE Trans. Nucl. Sci.*, vol. 54, no. 4, pp. 1319–1326, Aug. 2007.
- [14] R.-Y. Zhu, "Crystals for homogeneous hadron calorimeter," presented at the International Linear Collider Workshop 2008 at Chicago, [Online]. Available: http://www.hep.caltech.edu/~zhu/talks/ryz_081118_lcws.pdf
- [15] D. Shen *et al.*, *J. Inor. Mater.*, vol. 101, p. 11, 1995.
- [16] C. Woody *et al.*, in *Proc. SCINT95*, Delft, The Netherlands, 1996, Delft Univ. Press.
- [17] R. H. Mao, L. Y. Zhang, and R.-Y. Zhu, "A search for scintillation in doped cubic lead fluoride crystals," *IEEE Trans. Nucl. Sci.*, vol. 57, no. 6, pp. 3841–3845, Dec. 2010.
- [18] D. F. Anderson, M. Kobayashi, Y. Yoshimura, and C. L. Woody, "Lead fluoride: An ultracompact Cherenkov radiator for EM Calorimetry," *Nucl. Instrum. Meth.*, vol. A290, pp. 385–389.
- [19] 2nd Workshop for Material Development for the HHCAL Detector Concept. Beijing, May 9, 2010 [Online]. Available: <http://indico.ihep.ac.cn/sessionDisplay.py?sessionId=2&slotId=0&confId=1470#2010-05-09>
- [20] R. H. Mao *et al.*, "Precision crystal calorimeters in high energy physics: Past present and future," in *Proc. IX Int. Conf. Calorimetry in Particle Phys.*, B. Aubert, Ed. *et al.*, 2000, vol. XXI, Frascati Physics Series, pp. 709–720.
- [21] See presentations and papers in this conference.
- [22] H. Wenzel *et al.*, Simulation of a totally active dual read out calorimeter for future lepton colliders, FERMILAB-PUB-11-531-CD-E.
- [23] T. Kimble, M. Chou, and B. H. T. Chai, "It Scintillation properties of LYSO crystals," in *Proc. IEEE NSS Conf. Rec.*, 2002.
- [24] C. Woody *et al.*, "A study on the use of lead fluoride for electromagnetic calorimetry," *IEEE Trans. Nucl. Sci.*, vol. 40, no. 4, pp. 546–551, Aug. 1993.